Synthesis of ultra-narrow PbTe nanorods with extremely strong quantum confinement

Han, Lu; Fang, Honghua; Du, Chunmiao; Sun, Jianxia; Li, Youyong; Ma, Wanli

Published in:
Journal of Materials Science & Technology

DOI:
10.1016/j.jmst.2018.10.019

Publication date:
2019

Journal of Materials Science & Technology 35 (2019) 703–710

Contents lists available at ScienceDirect

Journal of Materials Science & Technology

journal homepage: www.jmst.org

Research Article

Synthesis of ultra-narrow PbTe nanorods with extremely strong quantum confinement

Lu Han [a], Honghua Fang [b], Chunmiao Du [a], Jianxia Sun [a], Youyong Li [a], Wanli Ma [a,*]

[a] Institute of Functional Nano & Soft Materials (FUNSOM), Soochow University, Suzhou, 215123, China
[b] Zernike Institute for Advanced Materials University of Groningen, Nijenborgh 4, Groningen, 9747 AG, the Netherlands

ARTICLE INFO

Article history:
Received 14 February 2018
Received in revised form 20 May 2018
Accepted 21 May 2018
Available online 24 October 2018

Keywords:
Colloidal semiconductor nanocrystals
PbTe nanorods
Optical properties

ABSTRACT

Monodisperse, high-quality, ultra-narrow PbTe nanorods were synthesized for the first time in a one-pot, hot-injection reaction using *trans*-2-decenoic acid as the agents for lead precursors and tris(diethylamino)phosphine telluride together with free tris(diethylamino)phosphine as the telluride precursors. High monomer reactivity, rapid nucleation and fast growth rate derived from the new precursors led to the anisotropic growth of PbTe nanocrystals at low reaction temperatures (<150 °C). In addition, the aspect ratio of PbTe nanorods could be largely adjusted from 4 to 15 by tuning the Pb to Te precursor molar ratio and reaction temperatures. Moreover, the synthesized ultra-narrow PbTe nanorods exhibited extremely strong quantum confinement and presented unique optical properties. We revealed that the diameter and length of PbTe nanorods could significantly affect their optical properties, which potentially offer them new opportunities in the application of optoelectronic and thermoelectric devices and make them desired subjects for multiple exciton generation and other fundamental physics studies.

1. Introduction

Colloidal semiconductor nanocrystals (NCs) with unique size- and shape-dependent electrical and optical properties, which intrinsically result from three-dimensional quantum confinement, have been exploited extensively in low-cost and solution-processed devices, such as field-effect transistors [1,2], solar cells [3–5], and light-emitting diodes [6]. In particular, one-dimensional (1D) semiconductor nanorods (NRs) and nanowires (NWs) are of significant interest for optoelectronic application owing to their linearly polarized emission [7], increased multiple exciton generation (MEG) [8,9] and enhanced carrier transport [10]. Designing ultra-narrow NRs with well dimensional homogeneity in the strong confinement regime is a challenge. Even then, the necessity for designing 1D semiconductor NRs of different materials is increasingly growing in order to understand the fundamental properties of materials and develop various electro-optical devices [11–13]. The increasing interest is particularly true for lead chalcogenides (Pb*E*, *E*=S, Se and Te), which can cover a very wide spectral range from mid-infrared to the visible region, yet have been investigated in 1D field to a lesser extent compared to cadmium chalcogenides [14–16]. Moreover, most of the II-VI and III-V class of NCs have a small Bohr radius and moderate difference in electron and hole effective masses, leading to weak quantum confinement and significant asymmetry between individual charge carriers. In comparison, lead chalcogenides have quite large Bohr radius, which allow one to achieve stronger confinement even with relatively larger dimensions. It was reported that ultra-narrow PbS NRs have the well-defined absorption peak and intense fluorescence in the visible region [15]. Recently, a maximum external quantum efficiency of 122% has been reported in PbSe NR solar cells, indicating a strong MEG effect [9].

Among lead chalcogenide systems, PbTe has a large excitonic Bohr radius (~ 46 nm) and light e^- and h^+ masses as well as a large dielectric constant (ε_0 ~ 1000), which make it widely used in photodetectors [17], solar cells [18], optical switches [19] and thermoelectrical devices [20]. In addition, the large anisotropy inherent to the bandstructure of PbTe ($a_{B\parallel}$ ~12 nm, $a_{B\perp}$ ~150 nm) renders PbTe NCs a uniquely interesting subject for optoelectronic investigations and shape engineering of quantum properties. Synthesizing PbTe NRs with high aspect ratio may provide the possibility showing quantum-confined effects in three dimensions. However, growing 1D PbTe NCs with a cubic crystal structure remains a big challenge because of the necessity to achieve a symmetry-breaking pathway for enabling anisotropic growth. So far, there are only a few reports regarding 1D PbTe NCs (such as

* Corresponding author.
E-mail address: wlma@suda.edu.cn (W. Ma).

https://doi.org/10.1016/j.jmst.2018.10.019
1005-0302/

NRs and NWs), which include sonoelectrochemical [21], hydrothermal [22], template-assisted [23], chemical vapor transport [24] and spark plasma sintering [25] synthesis. Recently, O'Brien et al. first reported a two-step colloidal method to synthesize PbTe NRs at temperature above 190 °C [26]. Nevertheless, the produced 1D PbTe NRs utilizing aforementioned methods have large diameters, which restricted the extent of quantum confinement. In addition, none of the these reports have shown the optical properties of the 1D PbTe NCs, likely due to the low solubility and shape nonuniformity of the synthesized NCs.

In this work, we report a simple, one-pot hot-injection synthesis of high-quality PbTe NRs and their shape-dependent optical properties. We largely improved the size and shape control of the synthesized PbTe NRs. Monodisperse ultra-narrow NRs with diameters < 5 nm has been successfully demonstrated by using *trans*-decenoic acid (*t*-2-DA) as the agents for lead precursors, and tris(diethylamino)phosphine telluride (TDPTe) together with free TDP as the telluride precursors. The new precursors lead to high monomer reactivity, rapid nucleation and fast growth rate, resulting in the anisotropic growth of PbTe NCs at relatively low reaction temperatures (<150 °C). What's more, tuning the Pb to Te precursor molar ratio and reaction temperatures can precisely control the aspect ratio of NRs, which can be varied from 4 to 15. The synthesized ultra-narrow PbTe NRs exhibit very strong quantum confinement and unique optical spectroscopy with three distinct excitonic absorption peaks, which have not been reported before. We believe that the interesting properties of these NRs can offer them opportunities for widespread application in optoelectronic devices.

2. Experimental

2.1. Materials

Lead oxide (99.9%), tellurium lump (99.999%), Tris(diethylamino)phosphine (TDP) (97%), oleic acid (tech., 90%) were purchased from Alfa-Aesar; *trans*-2-decenoic acid (*t*-2-DA) (>95%), *trans*-3-decenoic acid (*t*-3-DA) (>90%) were purchased from TCI; diphenylphosphine (DPP) (98%), 1-octadecene (ODE) (90%) were purchased from J&K; trimethyl phosphate (99%) were purchased from Sigma Aldrich. All chemicals were used without further purification unless noted. 1-Octadecene was dried by heating them to 100 °C under vacuum for 24 h and then placing them in a glovebox. A 1 M phosphine telluride solution was synthesized by mixing phosphine and Te lump overnight; the solution was stored in an inert-atmosphere glovebox.

2.2. PbTe nanorod synthesis

2.2.1. Control of reaction precursors in PbTe NR synthesis

All experiments were performed under a nitrogen atmosphere using standard air-free Schlenk line techniques. A solution of 0.4 mmol PbO (89 mg), 1 mmol carboxylic acid (oleic acid, *t*-2-DA and *t*-3-DA, respectively) and 8 g dried ODE were heated at 130 °C in a 50 ml three-neck flask under nitrogen. The solution was then degassed for an additional 1 h at 110 °C under vacuum before keeping the solution at 120 °C under nitrogen. Then a mixture of 1 M TDPTe solution (TDP: 0.12 ml TDPTe in 1.2 ml TDP and 1.2 ml ODE; DPP: 0.12 ml TDPTe in 1.2 ml TDP and 10 μl DPP in 1.2 ml ODE; ODE: 0.12 ml TDPTe in 2.4 ml ODE, respectively) was injected. The reaction was allowed to continue for 10 min, and then it was rapidly quenched by placing the flask in cold water and injecting 5 ml anhydrous hexane. The NCs were purified by precipitation twice in hexane/isopropanol (centrifuge at 8000 rpm for 5 min).

2.2.2. Control of Pb to Te precursor molar ratio in PbTe NR synthesis

A solution of 0.4 mmol PbO (89 mg), 1 mmol *t*-2-DA and 8 g dried ODE were heated at 130 °C in a 50 ml three-neck flask under nitrogen. The solution was then degassed for an additional 1 h at 110 °C under vacuum before keeping the solution at 120 °C under nitrogen. The Pb:Te precursor molar ratio was adjusted to specific values (20:3, 10:3, 10:9, 1:2 and 1:5, respectively) and then the volume of 1 M TDPTe can be varied from 0.06 to 2 ml. Then a mixture of 1 M TDPTe solution in 1.2 ml TDP and 1.2 ml ODE was injected. The reaction was allowed to run for 15 min before quenching the reaction.

2.2.3. Control of reaction temperature in PbTe NR synthesis

The Pb to Te precursor molar ratio was fixed at 20:3, while the PbTe NRs were grown at specific temperatures 100 °C, 120 °C and 140 °C. The growth time for PbTe NRs was allowed to run for 80 min. Size-selective precipitation could be carried out to obtain better monodispersity of NRs samples using hexane/isopropanol.

2.3. Characterization

TEM micrographs were taken using a Tecnai G2 F20 S-Twin transmission electron microsope. UV–vis-NIR spectra were recorded on a Perkin Elmer model Lambda 750. The second harmonic (400 nm) of a Ti:sapphire laser (Coherent, Mira 900, repetition rate 76 MHz) was used to excite the samples. The crystal structure of PbTe NCs was confirmed by XRD with an X'Pert-ProMPD (Holland) D/max-gAX-ray diffractometer with Cu Kα radiation (λ = 0.15406 nm). GIWAXS experiments were conducted at Shanghai Synchrotron Radiation Facility (SSRF) on diffraction beam line (BL14B1). The schematic diagram in Fig. S1 shows how to convert 2D GIWAXS to the out-of-plane spectra. For XRD and GIWAXS measurements, samples were prepared by depositing PbTe NC or NR solutions in chloroform onto a Si substrate. The IR spectra were recorded on an HYPERRION spectrometer with a pressed KBr pellet. ^{31}P-NMR data were performed on Varian Unity Inova 300 MHz spectrometer with trimethyl phosphate as the internal standard.

2.4. Theoretical calculation

All the first-principles calculations based on density functional theory (DFT) were performed with the DMol^3 package in Material Studio 7.0 from Accelrys Inc. The self-consistent all electron calculations were carried out by adopting a double numerical basis set including d-polarization functions (DND). The Perdew–Bruke–Ernzerhof (PBE) generalized gradient approximation (GGA) exchange-correlation energy term was chosen for all the structure optimization. The tolerance for energy and electron density in all the performed self-consistent field (SCF) computations was set as 10^{-5} a.u. A convergence criterion of 0.01 eV Å^{-1} for the forces was applied and a smearing value of 0.001 Ha in the orbital occupancy was used to speed up the convergence process. In order to obtain the total energy of the most stable structures, the entire related configurations have been fully optimized under the same conditions. In all the optimized structures at the atomic level, the energetic parameter (ΔE), which indicates the binding strength between the Pb cation and acid radical ion was calculated with the following expression:

$$\Delta E = \left(E_{\text{total}}(\text{Pb}(\text{XA})_2) - E_{\text{total}}(\text{Pb}) - 2E_{\text{total}}(\text{XA})\right)/2 \quad (1)$$

where $E_{\text{total(Pb(XA)2)}}$, $E_{\text{total(Pb)}}$ and $E_{\text{total(XA)}}$ represents the total energy of the optimized $\text{Pb}(\text{XA})_2$ structures, Pb cation and XA acid (oleic acid, *t*-2-DA and *t*-3-DA) molecules, respectively.

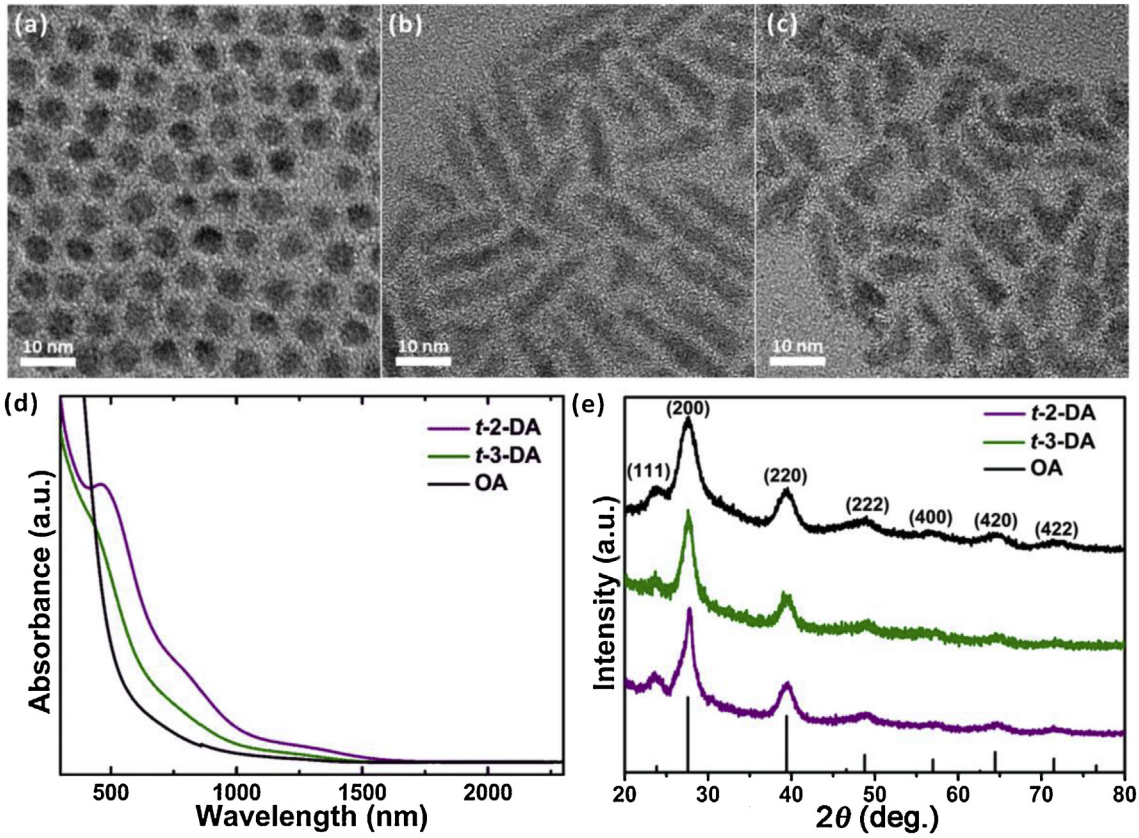

Fig. 1. (a–c) TEM images of PbTe NCs synthesized with oleic acid (OA) *trans*-2-decenoic acid (*t*-2-DA) and *trans*-3-decenoic acid (*t*-3-DA), respectively; (d) Normalized optical absorption spectra of PbTe NCs with different lead precursors; (e) WAXS patterns of corresponding PbTe NCs.

3. Results and discussion

3.1. Effect of different lead precursors on PbTe NC properties

In order to promote anisotropic growth of PbTe NCs, we used 1 M TDPTe dissolved in the mixture solution of TDP and 1-octadecene (ODE) as the telluride precursor. Here we chose three types of carboxylic acids including oleic acid (OA), *t*-2-DA and *trans*-3-decenoic acid (*t*-3-DA) as the agents for lead precursors (as seen in Fig. S2). The detailed dimension variations of PbTe NCs are shown in Fig. 1(a)–(c), with the parameters listed in Table S1. Apparently, spherical PbTe NCs were obtained by using OA, while one-dimensional PbTe NCs were synthesized with the use of short-chain carboxylic acid. Short ligand leads to fast growth and elongated NCs, which has also been observed in the synthesis of CdSe and PbSe NCs [27,28]. Interestingly, we found that the position of C=C bond in the decenoic acid can also influence PbTe NR morphology. Lower aspect ratio and much higher percentage of multiple branched NRs were obtained by using *t*-3-DA instead of *t*-2-DA. FTIR spectra of three free carboxylic acids and PbTe NCs coated with corresponding capping ligands are shown in Fig. S3. The results reveal that the ligands on the surface of PbTe NCs are the carboxylates, instead of free acids. The characteristic peaks of $-COO^-$ group are at 1636 cm^{-1} and 1560 cm^{-1} for both OA-PbTe and *t*-3-DA-PbTe samples, while those of $-COO^-$ are at 1650 cm^{-1} and 1548 cm^{-1} for *t*-2-DA-PbTe sample due to its π-π conjugated structure between C=C and C=O bond. In addition, we calculated the binding strength between Pb and three carboxylic acids by using computational modeling at the atomic level (see details in the Experimental Methods) and the related energetic parameters ΔE are listed in Table S2 and shown in Fig. S4. The value of ΔE for Pb-OA is lower than that for Pb-DA, suggesting a more stable binding. Meanwhile, the values of ΔE for Pb(*t*-2-DA) and Pb(*t*-3-DA) are equally high, which means that these precursors with similar bond strength can release more monomers than Pb-OA during nucleation stage and benefit the anisotropic growth of PbTe NCs.

Fig. 1(d) shows the room-temperature absorption spectra of PbTe NCs synthesized with three different lead precursors. The spherical PbTe NCs synthesized with OA shows no characteristic peak while PbTe NRs synthesized with *t*-3-DA has a broad excitonic peak around 440 nm. Surprisingly, PbTe NRs synthesized with *t*-2-DA shows a discrete sharp excitonic peak at 459 nm, a shoulder at 818 nm and a weak peak at 1276 nm. The sharp absorption peak of PbTe NRs is significantly blue-shifted compared to all previous reports on PbTe NCs [29–31], suggesting the extremely strong degree of confinement, which was also observed in ultra-narrow PbS NRs [15]. In addition, the wide-angle X-ray scattering (WAXS) spectra of corresponding PbTe NCs are displayed in Fig. 1(e). The spectra indicate that PbTe NCs using different lead precursors have the typical rock-salt structure (JCPDS: 38-1435), which are consistent with previously reported spectra for PbTe dots and rods [26]. PbTe NRs synthesized with *t*-2-DA or *t*-3-DA has a slightly narrower diffraction peak (200) than the spherical NCs using OA and the narrowest peak is observed when using *t*-2-DA. In addition, other peaks such as (222), (400), (420) and (422) can be observed, which were also reported in the previous literature [30]. These peaks are very weak due to the small diameters of our synthesized PbTe NCs, On the flat Si wafer, the elongated PbTe NRs align parallel to the substrate while the spherical NCs do not exhibit the preferred crystallographic orientation relative to the substrate (Fig. S5(a)). By using synchrotron-based grazing-incidence wide-angle X-ray scattering (GIWAXS), we further investigated and compared the difference of spherical NC and NR orientations on the substrates. As shown in the scattering spectra of PbTe QD and NR films

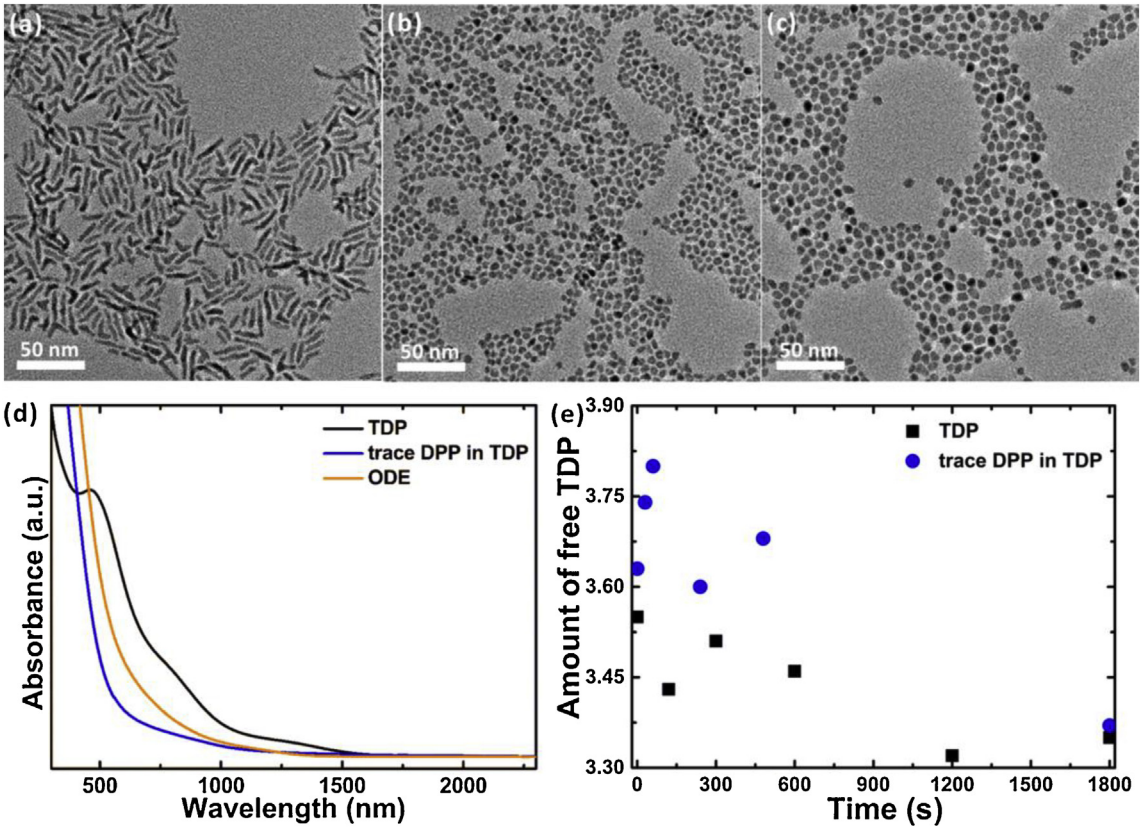

Fig. 2. TEM images of PbTe NCs synthesized with (a) 1 M TDPTe in the mixture solution of TDP and ODE, (b) trace DPP in the mixture solution of TDP and ODE, (c) as well as the ODE solution without TDP; (d) Normalized absorption spectra of the three PbTe NCs synthesized from the mixture solution of TDP and ODE (black line), trace DPP in the mixture solution (blue line), and ODE only solution (orange line); (e) Plot for the amount of free TDP for two different telluride precursors during reaction: black line represents the mixture solution of TDP and ODE; blue line represents trace DPP in the mixture solution. Data was obtained from integration of $^{31}P\{^{1}H\}$ NMR peaks.

(Fig. S5(b)–(d)), the (100) peak is more pronounced in the out-of-plane direction, which suggests NR growth in a favored direction and well-alignment on the substrate [32,33]. The finding confirms the anisotropy of PbTe NRs with *t*-2-DA. It also implies that NR growth is mainly in the [100] direction because the enhanced peak results from an increased number of lattice planes under the Bragg condition for diffraction, as Murray et al. reported the similar phenomenon in PbSe NRs [32].

3.2. *Effect of different telluride precursors on PbTe NC morphology*

Previously Christopher B. Murray et al. reported the role of different selenide precursors for PbSe NR synthesis and found that the presence of amine-based free phosphine in the Se precursor affected the morphology of PbSe NRs dramatically[34]. Here we also included amine-based phosphine in the telluride precursor for PbTe NR synthesis. The lead to telluride precursor molar ratio was set to 20:3 with 60 μl 1 M TDPTe (see more details in the Experimental Section). To obtain the optimal synthetic parameters for the control of PbTe NR morphology, we deliberately adjusted the composition of telluride precursor. TEM images show that using 1 M TDPTe dissolved in the mixture solution of TDP and ODE can produce PbTe NR (as seen in Fig. 2(a)–(c)). The synthesis without extra free TDP in telluride precursor forms only spherical products instead of NRs. According to previous reports, trace DPP added in the phosphine can greatly increase reactivity and promote the narrow rod growth [28]. However, in this work trace DPP added in the mixture solution results in uncontrollable reaction and irregular shapes of PbTe NCs. Given the above results, we conclude that free phosphine TDP has an important role in the morphology control of PbTe NRs. Meanwhile, the effect of trace DPP in telluride precursor works in a different way from that in PbSe NC synthesis. Absorption spectra also confirm the morphology-shaping effect of different telluride precursors. PbTe NRs synthesized using free TDP show absorption spectra with apparent peaks, while spherical NCs obtained by using trace DPP or ODE only solution exhibit no characteristic absorption peaks (as shown in Fig. 2(d)).

We performed $^{31}P\{^{1}H\}$ NMR to quantitatively detect the amount of free phosphine in different telluride precursors during PbTe synthesis. The molecular structure formulas of TDP, DPP and TDPTe present in Figs. S6 and S7 gives the reference $^{31}P\{^{1}H\}$ NMR data of 97% TDP, DPP as well as 1 M TDPTe. The chemical shift of free TDP is observed at around 118 ppm. Therefore, the chemical shift of reaction products at around 118 ppm can be recognized as the signal from free TDP while those at 125 ppm should be the signal from TDPTe (Fig. S8(a) and (b)). Then we used trimethyl phosphate (TMP) as the internal standard (chemical shift is around 3.0 ppm) to calculate the amount of free TDP under different conditions of PbTe synthesis. In the first synthesis scheme, only TDPTe was dissolved in the ODE solution as the telluride precursor. We observed no signal of free TDP released from TDPTe during reaction (Fig. S8(c)). In the second scheme, TDPTe and free TDP are both used in the telluride precursor, as shown in Fig. 2(e), the PbTe NR synthesis gradually consumes the free TDP which indicate that the anisotropic growth of PbTe NCs requires certain amount of free DPP. In the third synthesis scheme, with the addition of trace DPP in the mixture of TDPTe and free TDP, we observed a rapid increase in the amount of free TDP at the beginning and then the TDP signal decreased with elongated reaction time. The increased amount of free TDP may be from the decomposition of TDPTe due to the addition of DPP, which suggest

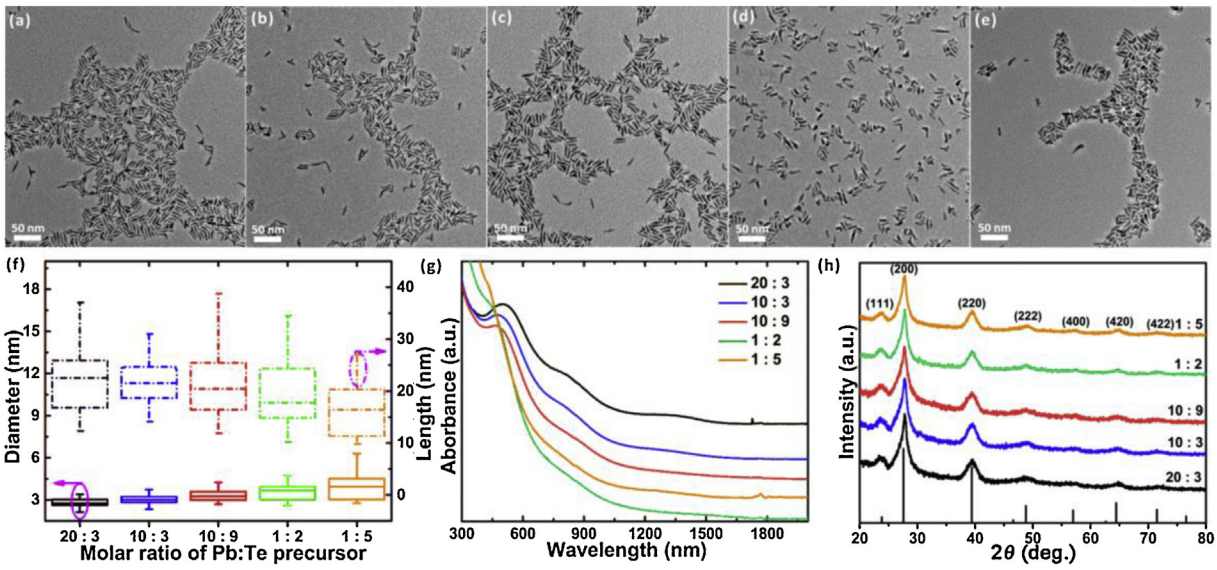

Fig. 3. (a–e) TEM images of PbTe NRs synthesized with the molar ratio of Pb:Te precursor of 20:3, 10:3, 10:9, 1:2 and 1:5, respectively; (f) Average diameter and length of the corresponding PbTe NRs synthesized with according Pb to Te precursor molar ratio; (g) Normalized absorption spectra of PbTe NRs synthesized with various Pb:Te molar ratios; (h) WAXS patterns of PbTe NRs synthesized with various Pb:Te molar ratios.

largely increased monomer concentration. As a result, the spherical PbTe NCs were obtained due to the great impact of DPP on enhancing NC nucleation and accelerating reaction rate [28,35–37]. Thus, we can conclude that the presence of free TDP truly participate in the nucleation and plays a critical role in morphology control of PbTe NR synthesis, which is consistent with the similar phenomena observed in PbSe NR synthesis [34].

3.3. Effect of precursor Pb to Te molar ratio on PbTe NR morphology

We investigated the effect of precursor Pb to Te molar ratio on PbTe NR morphology. In this experiment, we used *t*-2-DA as the agents for Pb precursor and 1 M TDPTe dissolved in the mixture solution of TDP and ODE as the Te precursor. Fig. 3(a)–(e) shows that the molar ratio of Pb/Te precursor can largely affect the morphology of the synthesized PbTe NRs at the same growth temperature. We chose five different molar ratio of 20:3, 10:3, 10:9, 1:2 and 1:5. With the molar ratio of 20:3, the NRs have an average diameter of 2.7 ± 0.2 nm and a length of 23 ± 4 nm. With further increasing Te precursor ratio, the diameter of PbTe NRs gradually increases to 3.9 ± 0.7 nm and the length decreases to 16 ± 3 nm, as shown in Fig. 3(f) and summarized in Table S3. The general trend is that the aspect ratio of NRs decreases as the Pb to Te precursor molar ratio decreases as listed in Table S3. These experimental data reveal that the telluride precursor, TDPTe, is more active than the lead precursor, Pb-(*t*-2-DA). As a result, the more telluride precursor exists in the initial stage of reaction, the faster the nucleation process occurs and the more the nuclei are generated in the nucleation stage. Consequently, the remaining amount of precursor monomers after the nucleation stage in the solution decreases significantly resulting in PbTe NRs with a lower aspect ratio.

The room-temperature absorption spectra of PbTe NRs synthesized with different molar ratios of Pb/Te precursor are given in Fig. 3(g). PbTe NRs with the largest Pb/Te molar ratio displays a well-defined excitonic absorption peak at around 496 nm, a shoulder at 824 nm and a weak peak at 1260 nm. When the molar ratio of Pb/Te precursor decreases from 10:3 to 10:9, the well-resolved excitonic absorption peak in the visible light region shifts from 476 to 470 nm. However, that discrete absorption peak vanishes as the Pb/Te molar ratio is below 10:9. Traditionally, the first excitonic absorption peak changes with size of NCs and most of the confinement is along the diameter in a rod or in a multipod-shaped NC, which has been demonstrated in previous literatures [14,32,38,39]. We also found that the smaller the diameters of PbTe NRs wre obtained, the more the discrete excitonic absorption peaks the NRs have. Up to now, studies of well-resolved optical absorption spectra from PbTe NRs have been still limited because of difficulties associated with preparing monodisperse PbTe NR samples and the more broadened excitonic transitions peaks of PbTe compared to other lead chalcogenides [29,30]. Nevertheless, our synthetic methods for PbTe NRs verify the hypothesis that PbTe NCs with a high aspect ratio has the possibility showing quantum-confined effects in three dimensions [30].

Fig. 3(h) displays the WAXS spectra of the corresponding PbTe NRs with specific Pb/Te precursor molar ratio. The spectra demonstrate that PbTe NRs with different aspect ratios share the same rock-salt structure (JCPDS: 38-1435). As the Pb/Te molar ratio decreases from 20:3 to 1:5, the corresponding (200) diffraction peak slowly broadens. The NRs with a large aspect ratio can easily align parallelly to the substrate. As a result, the larger aspect ratio PbTe NRs has, the narrower diffraction peak (200) of PbTe NRs is observed [28].

3.4. Impact of growth temperature on PbTe NRs

We explored the influence of growth temperature on the morphology of PbTe NRs with the optimized synthetic method. The TEM analysis of monodisperse PbTe NRs synthesized at growth temperatures of 100 °C, 120 °C and 140 °C are shown in Fig. 4. Low-magnification TEM images (Fig. 4(a)–(c)), which shows the uniformity of size and shape of NRs synthesized at various temperatures, reveal that the growth temperature has a great impact on PbTe NR morphology. Meanwhile, the single crystallinity and structural integrity of synthesized PbTe NRs at different growth temperatures are demonstrated by the high-resolution TEM (HRTEM) images (Fig. 4(d)–(f)). All the three PbTe NRs have the fringe spacing of 0.32 nm, which corresponds to the (200) lattice planes for the cubic rock salt structure of PbTe, as also reflected in the Fourier transform (insets). HRTEM images also

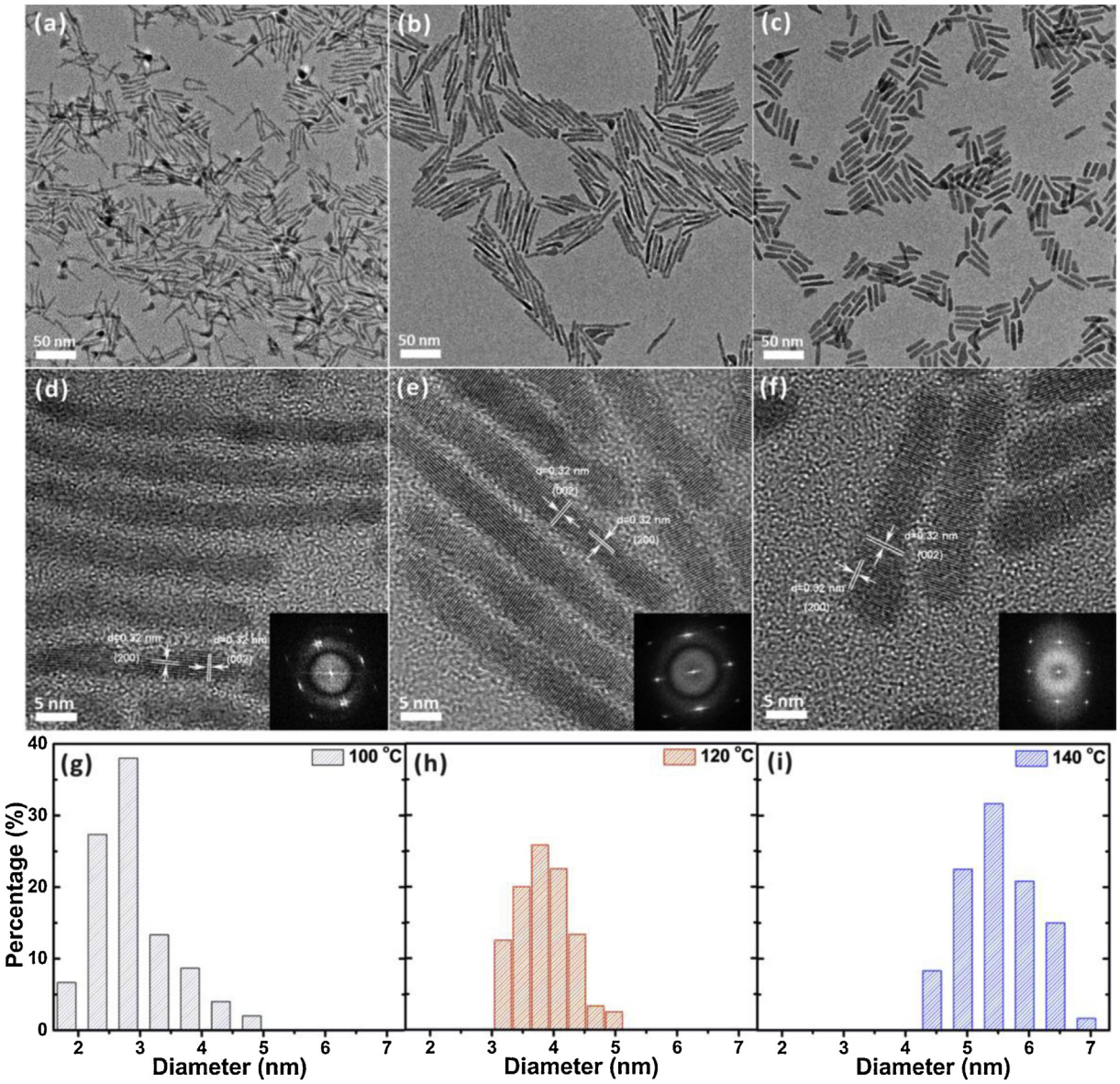

Fig. 4. (a–c) TEM and (d–f) HRTEM images of PbTe NRs synthesized at three different growth temperatures: 100 °C, 120 °C and 140 °C, respectively; (g–i) Diameter distribution histograms of corresponding PbTe NRs.

indicate that the [100] crystallographic axis is parallel to the long axis of the rods as previously described in anisotropic PbS and PbSe NCs [28,40]. Additionally, size statistics were measured from TEM images using NanoMeasurer software. For each samples, the diameters and lengths of more than 100 NRs were measured. The diameter distributions are shown in Fig. 4(g)–(i), which exhibits that the diameters of PbTe NRs increase with raising growth temperature. And the NRs with the highest uniformity have an average diameter of 3.8 ± 0.4 nm at the growth temperature of 120 °C. Nevertheless, the average NR length follows a more complex trend and the longest NRs are achieved at the median growth temperature of 120 °C (Fig. S9). The detailed dimensions of PbTe NRs are listed in Table S4. The shortest PbTe NRs are obtained at 140 °C, which may be derived from the rapid consumption of precursors and the formation of more nuclei at nucleation stage. Then subsequently Oswald ripening happens in the later reaction stage as a result of exhaustion of the precursors. In brief, we can fine control the diameters, lengths and thereby aspect ratios of PbTe NRs by adjusting the growth temperature.

Comparing the optical properties of above PbTe NRs with high uniformity may provide insight into their electronic structure and properties. Fig. 5(a) compares the room-temperature absorption spectra of PbTe NRs synthesized at different growth temperatures. All NR colloidal solutions have three excitonic peaks from visible to near infrared absorption region. It is known that bulk PbTe has a direct band gap of 0.23 eV and a very large average excitonic Bohr radius (~ 46 nm), leading to extremely strong quantum confinement. In addition, Murphy et al. reported the large anisotropy inherent to the bandstructure of PbTe ($a_{B\parallel} \sim 12$ nm, $a_{B\perp} \sim 152$ nm), which is most pronounced among the lead chalcogenide systems, compared to 66 nm for PbSe and 23.5 nm for PbS [29]. Therefore, our synthesized PbTe NRs with different lengths may present quantum-confinement effects in three dimensions and reveal how their anisotropic properties affect the optoelectronic properties of PbTe NCs [41]. In the near infrared region, the first excitonic absorption peak of PbTe NRs red-shifts from 1182 to 1713 nm as the average diameter of corresponding NRs increases from 2.8 to 5.4 nm (Fig. 5(b)), which is commonly observed in colloidal semi-

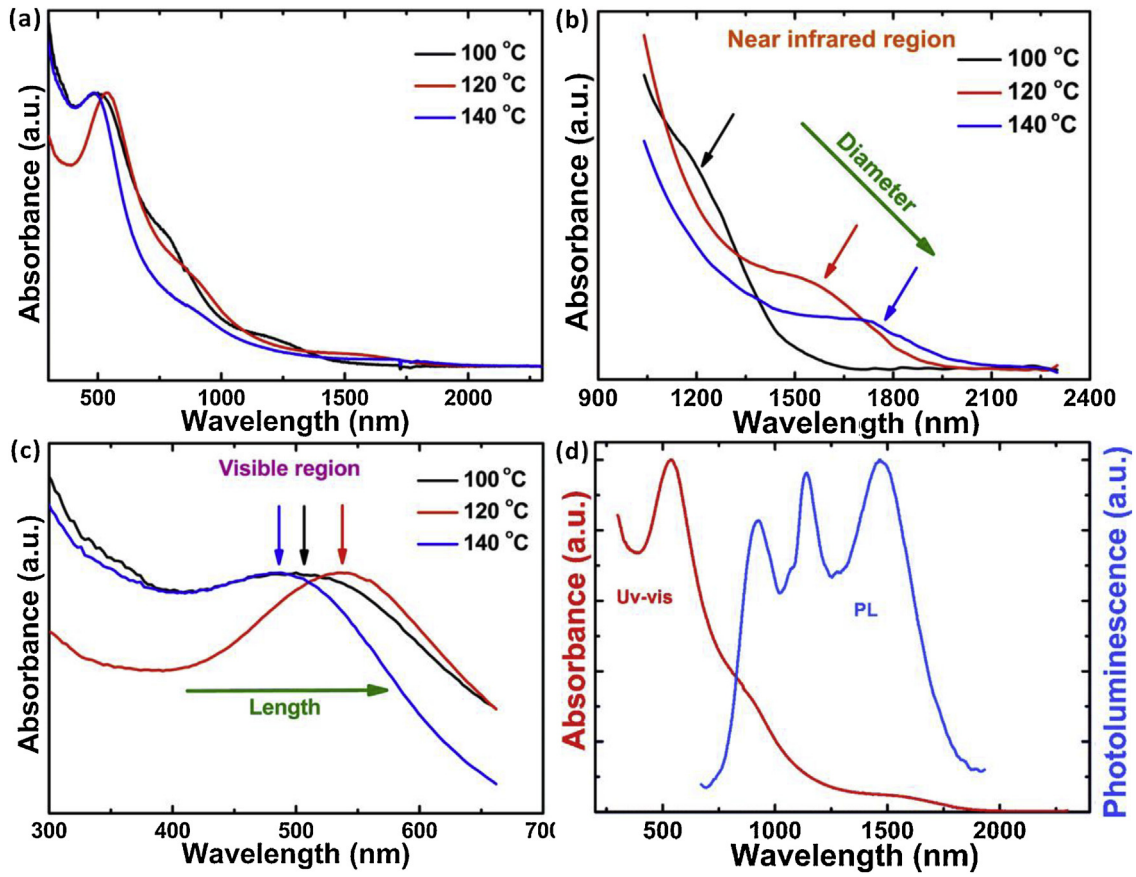

Fig. 5. (a) Normalized absorption spectra of PbTe NRs synthesized at 100 °C, 120 °C, 140 °C respectively; (b) Near infrared region and (c) visible region in PbTe NR absorption spectra; (d) Absorption (red solid curves) and PL (blue solid curves, excitation wavelength 400 nm) spectra for PbTe NRs synthesized at 120 °C.

conductor NCs [14,28,38,39]. But the first exciton absorption peaks of monodisperse PbTe NRs are much broader compared with those reported in spherical NCs [29,30]. The slightly larger size dispersion of PbTe NRs may not be the only reason for the observed peak broadening. Whereas in visible region, the discrete excitonic absorption peak of NRs at 487 nm (synthesized at 140 °C) gradually red shifts from 500 nm (100 °C) to 540 nm (120 °C) with increasing length of the NRs but smaller diameters, as shown in Fig. 5(c). It can be explained by that the anisotropy of the PbTe bandstructure prones to perturb the higher-energy state more so than the lowest-energy state, which has been demonstrated by Tudury et al. [42]. Currently, we speculate that these unique physical properties of PbTe NRs originate in both band mixing and the extreme anisotropy of the PbTe bandstructure near its 4-fold degenerate L point, which spread out the oscillator strengths over a wide energy range [42,43]. However, it has proven difficult to treat with great precision theoretically and is still not entirely understood.

Fig. 5(d) exhibits the room temperature absorption and PL spectra of PbTe NRs with the highest aspect ratio of ~15, which are synthesized at the growth temperature of 120 °C. The absorption spectra show discrete sharp excitonic bands at 540 nm (2.30 eV) with a narrow FWFM of 125 nm, a shoulder at 860 nm (1.44 eV) and a weak first exciton band at 1462 nm (0.85 eV). The PL spectrum shows strong and sharp emissions at 923 nm, 1139 nm and 1468 nm, respectively. According to the former report on ultra-narrow PbS NRs with only 1.7 nm diameter, their PL photoluminescence exhibit discrete sharp excitonic bands at 278 nm, 315 nm and 365 nm [15]. Our similar observation in ultra-narrow PbTe NRs is consistent with their results [44]. To the best of our knowledge, this study presents the first optical characterization of monodisperse PbTe NRs with the highest aspect ratio ~15 and thus provides the opportunity to show the well-resolved excitonic transitions in PbTe material.

4. Conclusion

We report for the first time a low-temperature, hot-injection synthesis of high-quality ultra-narrow PbTe NRs by introducing *t*-2-DA as the capping agents for lead precursors and TDPTe dissolved in excess TDP as the telluride precursors. The new synthesis scheme results in high monomer reactivity, rapid nucleation and fast growth rate, leading to the anisotropic growth of PbTe NCs at very low reaction temperature (< 150 °C). The control of PbTe NR aspect ratio can be implemented by tuning the Pb to Te precursor molar ratio or changing growth temperature. As a consequence, PbTe NRs ranging in small diameter from 2.7 to 5.4 nm and high aspect ratio from ~ 4 to ~15 are reported. Due to the large Bohr radius and electronic band anisotropy of PbTe, these NRs exhibit very strong quantum confinement confirmed by their rich features in optical spectroscopy. We believe that these ultra-narrow PbTe NRs may find new opportunities in the application of optoelectronic and thermoelectric devices and become a desired subject for multiple exciton generation and other fundamental physics studies.

Acknowledgements

This work was financially supported by the National Key Research Projects (No. 2016YFA0202402), the Natural Science Foundation of Jiangsu Province of China (No. BK20170337), the

National Natural Science Foundation of China (No. 61674111), “111” projects and the Priority Academic Program Development of Jiangsu Higher Education Institutions (PAPD). L. Han thanks State-Sponsored Scholarship for Graduate Students from China Scholarship Council (No. 201606920064).

Appendix A. Supplementary data

Supplementary material related to this article can be found, in the online version, at doi:https://doi.org/10.1016/j.jmst.2018.10.019.

References

[1] M.I. Nugraha, H. Matsui, S. Watanabe, T. Kubo, R. Häusermann, S.Z. Bisri, M. Sytnyk, W. Heiss, M.A. Loi, J. Takeya,Adv. Electron. Mater. 3 (2017), 1600360.
[2] L. Han, D.M. Balazs, A.G. Shulga, M. Abdu-Aguye, W. Ma, M.A. Loi,Adv. Electron. Mater. 4 (2018), 1700580.
[3] M. Liu, O. Voznyy, R. Sabatini, F.P. Garcia de Arquer, R. Munir, A.H. Balawi, X. Lan, F. Fan, G. Walters, A.R. Kirmani, S. Hoogland, F. Laquai, A. Amassian, E.H. Sargent, Nat. Mater. 16 (2017) 258–263.
[4] Z. Zhang, Z. Chen, L. Yuan, W. Chen, J. Yang, B. Wang, X. Wen, J. Zhang, L. Hu, J.A. Stride, G.J. Conibeer, R.J. Patterson, S. Huang,Adv. Mater. 29 (2017), 1703214.
[5] G. Shi, Y. Wang, Z. Liu, L. Han, J. Liu, Y. Wang, K. Lu, S. Chen, X. Ling, Y. Li, S. Cheng, W. Ma,Adv. Energy Mater. 7 (2017), 1602667.
[6] X. Yang, F. Ren, Y. Wang, T. Ding, H. Sun, D. Ma, X.W. Sun, Sci. Rep. 7 (2017) 14741.
[7] J. Hu, L. Li, W. Yang, L. Manna, L. Wang, A.P. Alivisatos, Science 292 (2001) 2060–2063.
[8] P.D. Cunningham, J.E. Boercker, E.E. Foos, M.P. Lumb, A.R. Smith, J.G. Tischler, J.S. Melinger, Nano Lett. 11 (2011) 3476–3481.
[9] N.J. Davis, M.L. Bohm, M. Tabachnyk, F. Wisnivesky-Rocca-Rivarola, T.C. Jellicoe, C. Ducati, B. Ehrler, N.C. Greenham, Nat. Commun. 6 (2015) 8259.
[10] H.C. Chen, C.W. Lai, I.C. Wu, H.R. Pan, I.W.P. Chen, Y.K. Peng, C.L. Liu, C.H. Chen, P.T. Chou, Adv. Mater. 23 (2011) 5451–5455.
[11] X. Fang, T. Zhai, U.K. Gautam, L. Li, L. Wu, Y. Bando, D. Golberg, Prog. Mater. Sci. 56 (2) (2011) 175–287.
[12] Y.N. Zhu, G.H. Zheng, Z.X. Dai, J.J. Mu, Z.F. Yao, J. Mater. Sci. Technol. 33 (8) (2017) 834–842.
[13] Z. Li, Y. Huang, X. Wang, D. Wang, X. Wang, F. Han, J. Mater. Sci. Technol. 33 (8) (2017) 864–868.
[14] W. Ma, S.L. Swisher, T. Ewers, J. Engel, V.E. Ferry, H.A. Atwater, A.P. Alivisatos, ACS Nano 5 (2011) 8140–8147.
[15] S. Acharya, U.K. Gautam, T. Sasaki, Y. Bando, Y. Golan, K. Ariga, J. Am. Chem. Soc. 130 (2008) 4594–4595.
[16] H. Choi, J.H. Ko, Y.H. Kim, S. Jeong, J. Am. Chem. Soc. 135 (2013) 5278–5281.
[17] Z. Lin, M. Wang, L. Zhang, Y. Xue, X. Yao, H. Cheng, J. Bai, J. Mater. Chem. 22 (2012) 9082–9085.
[18] M.L. Bohm, T.C. Jellicoe, M. Tabachnyk, N.J. Davis, F. Wisnivesky-Rocca-Rivarola, C. Ducati, B. Ehrler, A.A. Bakulin, N.C. Greenham, Nano Lett. 15 (2015) 7987–7993.
[19] E. Rodriguez, G. Kellermann, A.F. Craievich, E. Jimenez, C.L. César, L.C. Barbosa, Superlattices Microstruct. 43 (2008) 626–634.
[20] H. Fang, Z. Luo, H. Yang, Y. Wu, Nano Lett. 14 (2014) 1153–1157.
[21] X. Qiu, Y. Lou, A.C. Samia, A. Devadoss, J.D. Burgess, S. Dayal, C. Burda, Angew. Chem. Int. Ed. 44 (2005) 5855–5857.
[22] L. Zhang, J.C. Yu, M. Mo, L. Wu, K.W. Kwong, Q. Li, Small 1 (2005) 349–354.
[23] A. Purkayastha, Q. Yan, D.D. Gandhi, H. Li, G. Pattanaik, T. Borca-Tasciuc, N. Ravishankar, G. Ramanath, Chem. Mater. 20 (2008) 4791–4793.
[24] M. Fardy, A.I. Hochbaum, J. Goldberger, M.M. Zhang, P. Yang, Adv. Mater. 19 (2007) 3047–3051.
[25] S.W. Finefrock, G. Zhang, J.-H. Bahk, H. Fang, H. Yang, A. Shakouri, Y. Wu, Nano Lett. 14 (2014) 3466–3473.
[26] N. Ziqubu, K. Ramasamy, P.V.S.R. Rajasekhar, N. Revaprasadu, P. O'Brien, Chem. Mater. 22 (2010) 3817–3819.
[27] W. Wang, S. Banerjee, S.G. Jia, M.L. Steigerwald, I.P. Herman, Chem. Mater. 19 (2007) 2573–2580.
[28] L. Han, J. Liu, N. Yu, Z. Liu, J. Gu, J. Lu, W. Ma, Nanoscale 7 (2015) 2461–2470.
[29] J.E. Murphy, M.C. Beard, A.G. Norman, S.P. Ahrenkiel, J.C. Johnson, P. Yu, O.I. Mićić, R.J. Ellingson, A.J. Nozik, J. Am. Chem. Soc. 128 (2006) 3241–3247.
[30] J.J. Urban, D.V. Talapin, E.V. Shevchenko, C.B. Murray, J. Am. Chem. Soc. 128 (2006) 3248–3255.
[31] D.-K. Ko, C.B. Murray, ACS Nano 5 (2011) 4810–4817.
[32] W.K. Koh, A.C. Bartnik, F.W. Wise, C.B. Murray, J. Am. Chem. Soc. 132 (2010) 3909–3913.
[33] K.-S. Cho, D.V. Talapin, W. Gaschler, C.B. Murray, J. Am. Chem. Soc. 127 (2005) 7140–7147.
[34] W.K. Koh, Y. Yoon, C.B. Murray, Chem. Mater. 23 (2011) 1825–1829.
[35] K. Yu, X. Liu, Q. Zeng, D.M. Leek, J. Ouyang, K.M. Whitmore, J.A. Ripmeester, Y. Tao, M. Yang, Angew. Chem. Int. Ed. 52 (2013) 4823–4828.
[36] J.L. Peters, K.H.W. van den Bos, S. Van Aert, B. Goris, S. Bals, D. Vanmaekelbergh, Chem. Mater. 29 (2017) 4122–4128.
[37] X. Zhu, Z. Liu, G. Shi, J. Gu, W. Wang, W. Ma, J. Mater. Sci. Technol. 33 (2017) 418–423.
[38] M.A. Hines, G.D. Scholes, Adv. Mater. 15 (2003) 1844–1849.
[39] L. Manna, D.J. Milliron, A. Meisel, E.C. Scher, A.P. Alivisatos, Nat. Mater. 2 (2003) 382–385.
[40] S. Kundu, J.P. Hill, G.J. Richards, K. Ariga, A.H. Khan, U. Thupakula, S. Acharya, ACS Appl. Mater. Int. 2 (2010) 2759–2766.
[41] D. Debellis, G. Gigli, S. Ten Brinck, I. Infante, C. Giansante, Nano Lett. 17 (2017) 1248–1254.
[42] G.E. Tudury, M.V. Marquezini, L.G. Ferreira, L.C. Barbosa, C.L. Cesar, Phys. Rev. B 62 (2000) 7357–7364.
[43] F.W. Wise, Acc. Chem. Res. 33 (2000) 773–780.
[44] A.C. Berends, C. de Mello Donega, J. Phys. Chem. Lett. 8 (2017) 4077–4090.